nature

https://doi.org/10.1038/s41586-026-11368-9

Accelerated Article Preview

Carbon radical generation by irreversible metal-to-ligand charge transfer

Received: 14 April 2026

Accepted: 28 October 2026

Accelerated Article Preview
Published online: 04 November 2026

Cite this article as: Wei, Z. et al.
Carbon radical generation by irreversible metal-to-ligand charge transfer. *Nature*
https://doi.org/10.1038/s41586-026-11368-9
(2026)

Zhiqiang Wei, Xiang Li, Lin Xiao, Yu He, Zhao Liu, Kaidi Zhu, Chuanfa Ni, Xiao-Song Xue & Jinbo Hu

This is a PDF file of a peer-reviewed paper that has been accepted for publication. Although unedited, the content has been subjected to preliminary formatting. Nature is providing this early version of the typeset paper as a service to our authors and readers. The text and figures will undergo copyediting and a proof review before the paper is published in its final form. Please note that during the production process errors may be discovered which could affect the content, and all legal disclaimers apply.

ACCELERATED ARTICLE PREVIEW

Carbon radical generation by irreversible metal-to-ligand charge transfer

Zhiqiang Wei[1,2,3], Xiang Li[1,3], Lin Xiao[1,3], Yu He[1,3], Zhao Liu[1], Kaidi Zhu[1], Chuanfa Ni[1], Xiao-Song Xue*[1] & Jinbo Hu*[1,2]

[1]State Key Laboratory of Fluorine and Nitrogen Chemistry and Advanced Materials, Shanghai Institute of Organic Chemistry, University of Chinese Academy of Sciences, Chinese Academy of Sciences, 345 Ling-Ling Road, Shanghai 200032, China.
[2]School of Physical Science and Technology, ShanghaiTech University, 100 Haike Road, Shanghai 201210, China.
[3]These authors contributed equally: Zhiqiang Wei, Xiang Li, Lin Xiao, Yu He.
*Corresponding author emails: jinbohu@sioc.ac.cn (J.H.); xuexs@sioc.ac.cn (X.-S.X.)

Metal-to-ligand charge transfer (MLCT) is a fundamental photoinduced process that underpins a broad range of energy- or electron-transfer events[1,2]. In the absence of productive substrate engagement, the MLCT excited state typically relaxes to the ground state via photophysical deactivation, reflecting its largely reversible character[3,4]. Here we report a class of isolable copper–heteroaryl sulfone complexes that, upon visible light irradiation, undergo an irreversible MLCT-driven fragmentation through C–S bond cleavage within the coordinated sulfone ligand, generating carbon-centered radicals. Spectroscopic and computational studies support the formation of MLCT-derived excited states and a low-barrier pathway for C–S bond cleavage. This reactivity is largely independent of the reduction potentials of the corresponding free sulfones, enabling the generation of fluoroalkyl and non-fluorinated tertiary, secondary, and primary (even methyl) alkyl radicals. We demonstrate the utility of this platform in copper-catalyzed C–H fluoroalkylation of arenes and terminal alkynes. Leveraging these MLCT-generated trifluoromethyl radicals to initiate halogen-atom transfer (XAT) from perfluorocyclobutyl iodide (I-FCB), we also achieve radical perfluorocyclobutylation–iodination of alkenes, addressing a longstanding challenge in the incorporation of perfluorocyclobutyl motifs.

Metal-to-ligand charge transfer (MLCT) is a fundamental photoinduced process in coordination chemistry and underpins a broad range of photochemical and photocatalytic transformations[1,2]. In an MLCT process, electron transfer from metal-based orbitals to antibonding (usually π*) orbitals on the ligand framework generates a charge-separated excited state with redox activity[5]. However, in the absence of external reactants, most MLCT excited states undergo rapid photophysical deactivation back to the ground state, reflecting the reversibility of this process

ACCELERATED ARTICLE PREVIEW

(Fig. 1a, i). Although a few studies have revealed the ligand dissociation and release of neutral molecules following MLCT excitation (Fig. 1a, ii)[3,4], and radical generation from photoexcited metal complexes has recently been achieved, the latter systems require prior reduction of the complex by an external reductant before photoinduced bond cleavage can occur[6]. Thus, direct generation of synthetically useful carbon-centered radicals through fragmentation of coordinated substrates driven by an intrinsic MLCT process remains elusive (Fig. 1a, iii).

Fig. 1 | **Addressing the challenge of irreversible metal-to-ligand charge transfer (MLCT)**. **a**, Divergent pathways from MLCT excited states (A. excited-state formation; B. photophysical relaxation; C. ligand fragmentation). **b**, Reaction design. **c**, Irreversible MLCT-initiated perfluoroalkylation-iodination of alkenes. X, heteroatom or carbon; R, alkyl group; M, metal; L, ligand; SET, single-electron transfer; XAT, halogen-atom transfer; Alkyl, alkyl group.

At a fundamental level, MLCT excited states tend to relax back to the ground state because the ligand-centered radical anion generated upon photoexcitation is generally stable and lacks a driving force for bond cleavage or further irreversible chemical transformation[7]. By contrast, direct-photoexcitation platforms based on preassembled precursors, including ligand-to-metal charge transfer (LMCT)[8,9] systems, electron donor–acceptor (EDA) complexes[10,11], alkyl-1,4-dihydropyridines (DHPs)[12], and organoborate complexes[13], generate highly reactive charge-separated excited states in which photoinduced charge transfer is directly coupled to bond fragmentation, enabling efficient radical generation without the need for an external photocatalyst. Therefore, enabling radical generation from MLCT excited states requires direct coupling of photoinduced charge transfer to bond cleavage. Guided by this design principle, and inspired by our previous studies[14,15], we identified heteroaryl alkyl sulfones as particularly attractive candidates because they can coordinate to metal centers and, crucially, undergo irreversible reduction accompanied by C–S bond cleavage. Equally important, the metal center itself must be incapable of reducing such sulfones, thereby preventing spontaneous ground-state electron transfer. In our prior work, although iron catalysts were found to promote this reduction, their strong reducing character led to ultrafast electron transfer, precluding the isolation and structural characterization of the corresponding complexes[15]. Copper, by contrast, offers a

ACCELERATED ARTICLE PREVIEW

fundamentally different redox landscape: its comparatively weaker reducing power suppresses spontaneous ground-state electron transfer[16-20], enabling the stabilization and isolation of well-defined copper–heteroaryl sulfone complexes. We reasoned that such complexes could function as dormant precursors that, upon visible-light excitation, access an MLCT manifold redirected away from photophysical reversibility and toward irreversible ligand fragmentation and radical release (Fig. 1b).

Building on these design principles, we report a class of isolable copper-heteroaryl sulfone complexes that undergo visible-light-induced MLCT followed by rapid ligand fragmentation to generate a diverse range of alkyl radicals. Coordination of the sulfone to the copper center enables a photoactive MLCT pathway that is distinct from outer-sphere reduction of the corresponding free sulfone. As a result, the reduction potentials of the free sulfones alone do not predict their radical-generation behavior in the coordinated state. This strategy enables the generation of both fluoroalkyl and non-fluorinated alkyl radicals, including tertiary, secondary and primary (even methyl) alkyl radicals. We further exploit the resulting trifluoromethyl radical as an initiator for iodine-atom transfer from perfluorocyclobutyl iodide (I-FCB), enabling a radical perfluorocyclobutylation–iodination of alkenes and providing an efficient approach to the challenging incorporation of perfluorocyclobutyl motifs (Fig. 1c). More broadly, this strategy redirects the fate of MLCT excited states from photophysical deactivation (reversible pathway) toward the productive bond cleavage and radical generation (irreversible pathway).

Fig. 2 | **Characterization and reactivity investigation of the isolated copper(I)-sulfone complexes**. **a**, Preparation of copper(I)-sulfone complexes with sulfone **1a** and **1b**. **b**, Preparation of copper(I)-sulfone complex with sulfone **1c**. **c**, Stoichiometric reactions of complex **Cu-2** under blue LEDs irradiation in CH_2Cl_2; **d**, UV–vis absorption spectra of various compounds in CH_2Cl_2; **e**, Femtosecond transient absorption spectroscopy of **Cu-2** in CH_2Cl_2; **f**, Light on/off control experiment for **Cu-2** decomposition. rt, room temperature.

Although the relatively weak reducing power of copper in the ground state suppresses spontaneous electron transfer, copper complexes are susceptible to Jahn–Teller distortion upon photoexcitation into the MLCT state, drastically truncating the excited-state lifetime[21]. The use of bulky and rigid bisphosphine ligands inhibits this structural deformation, preserving the MLCT

ACCELERATED ARTICLE PREVIEW

character and enabling productive ligand fragmentation[21]. With this design principle in mind, we selected DPEphos as the ligand to suppress Jahn–Teller distortion and employed trifluoromethyl-substituted heteroaryl sulfones as the cleavable ligand, which are among the most susceptible alkyl sulfones to single-electron transfer (SET) and subsequent radical generation[14,22]. Although a mixture of **Cu-1** and **1a** generated trifluoromethyl radicals upon visible-light irradiation (Fig. 2a and Table S10), we were unable to isolate single crystals of the corresponding complex.

Inspired by previous reports of copper complexes supported by bis(heteroaryl) sulfone ligands[23], we next examined sulfone **1b** as a candidate to displace acetonitrile from the copper center. Although a mixture of **Cu-1** (Extended Data Fig. 1a) and **1b** generated trifluoromethyl radicals upon visible-light irradiation (Table S10), this strategy likewise failed to afford single crystals of the corresponding complex (Fig. 2a). We therefore reasoned that increasing the number of potential coordination sites might facilitate ligand exchange. Accordingly, a symmetrical heteroaryl sulfone **1c** was employed to replace the acetonitrile ligand in **Cu-1**, successfully affording the single crystals of copper complex **Cu-2** (Fig. 2b and Extended Data Fig. 1b). Notably, and contrary to our initial design, coordination occurs through only one side of the sulfone ligand, with both the nitrogen and oxygen atoms binding to the copper center, while the other side of sulfone unit remains non-coordinating (Extended Data Fig. 1b).

The reactivity of **Cu-2** was next examined (Fig. 2c). The complex **Cu-2** remained stable for over three years under ambient conditions in the dark, with only a 2% decrease (as detected by fluorine-19 nuclear magnetic resonance (^{19}F NMR) spectroscopy), indicating that Cu(I) alone is insufficient to efficiently activate trifluoromethyl sulfone **1c** (see Fig. S21). In stark contrast, blue light irradiation—either in CH_2Cl_2 solution or in the solid state—induces MLCT, promoting electron transfer from Cu(I) to the sulfone moiety to generate Cu(II), followed by C–S bond cleavage to afford a trifluoromethyl radical and a sulfinate anion. The formation of Cu(II) (Extended Data Fig. 1c) was confirmed by electron paramagnetic resonance (EPR) spectroscopy[24,25]. Upon irradiation of **Cu-2** in CH_2Cl_2 for 2 min, measurements at 100 K revealed pronounced g-factor anisotropy ($g_{x,y,z}$ = [2.04, 2.14, 2.33]), consistent with localization of the unpaired electron in the d(x^2–y^2) orbital. The corresponding hyperfine coupling constants ($A_{x,y,z}$ = [154, 168, 336] MHz) further corroborate the characteristic electronic structure of Cu(II), in good agreement with theoretical calculations. Formation of the trifluoromethyl radical was further supported by efficient trapping with TEMPO (Fig. 3a). As Cu(II) is known to undergo reduction to Cu(I) in the presence of phosphine ligands[26], the copper species ultimately isolated

ACCELERATED ARTICLE PREVIEW

and characterized by single-crystal X-ray diffraction was **Cu-3** (Extended Data Fig. 1d), a Cu(I) complex bearing a coordinated sulfinate ligand (Fig. 2c).

We next investigated the absorption spectra of the above species (Fig. 2d). Neither **Cu-1** nor DPEphos exhibited appreciable absorption in the visible region. In contrast, upon mixing **Cu-1** with **1a**, **1b**, or **1c**, new absorption bands extending into the visible region were observed in all cases. Moreover, each mixture released trifluoromethyl radicals under visible-light irradiation, indicating that our strategy is not restricted to a specific sulfone substrate. Notably, the visible-light absorption of **Cu-2** was substantially stronger than that of the corresponding in situ generated complexes, suggesting that coordinating species such as CH_3CN interfere with the coordination between **Cu-1** and the *N*-heteroaryl sulfones, thereby suppressing the in-situ formation of Cu-sulfone complexes. Transient absorption spectroscopy revealed an excited-state lifetime of 8.5 ns for **Cu-2**, which is consistent with an MLCT excited state in copper complexes[21]. Furthermore, a pronounced transient absorption band was observed in the 500–600 nm region, consistent with the formation of a ligand-centered radical anion following MLCT excitation (Fig. 2e)[21].

For deeper insights into the photoinduced radical generation process, DFT and time-dependent DFT (TD-DFT) calculations were performed on the frontier orbitals of **Cu-2** and its photo-excitation process, respectively. The frontier molecular orbitals of **Cu-2** are shown in Extended Data Fig. 2a. The HOMO is primarily located over the phosphorus atoms and the central Cu atom, indicating that it is mainly associated with the Cu−P coordination bonds of the Cu(DPEphos) fragment of **Cu-2**. In contrast, the LUMO is delocalized over the pyrimidine ring of sulfone **1c** and corresponds to its π* orbital. TD-DFT calculations show that the HOMO → LUMO excitation dominates the S_1 excited state, accounting for 84.8% of the electronic transition. This HOMO → LUMO excitation corresponds to charge transfer from the Cu(DPEphos) fragment to the coordinated sulfone **1c**, as further confirmed by hole–electron analysis[27] (Extended Data Fig. 2b). The hole is predominantly localized on the Cu center, contributing 53.5% of the hole density, whereas the excited electron is mainly distributed over the pyrimidine π* orbital of coordinated sulfone **1c**. Therefore, excitation to **Cu-2-S_1** corresponds to electron transfer from the Cu(DPEphos) fragment to the coordinated sulfone **1c**, indicating that **Cu-2-S_1** is best described as an MLCT state.

ACCELERATED ARTICLE PREVIEW

Fig. 3 | **MLCT-enabled alkylation**. **a**, MLCT-enabled generation of alkyl radicals; **2**, **3**, **4**, **6**-**11**, NMR yield; **5**, GC yield. **b**, MLCT-enabled alkylation of alkenes. **c**, **Cu-complex**-enabled trifluoromethyl- and difluoromethyl-azidation of alkenes. **d**, **Cu-complex**-catalyzed fluoroalkylation of arenes. Sulfones **1c** and **1d** are used, respectively. **e**, MLCT-enabled and copper-catalyzed fluoroalkylation of terminal alkynes. Unless otherwise mentioned, the yields refer to isolated yields. TEMPO, 2,2,6,6-Tetramethylpiperidin-1-oxyl; Ad, 1-adamantyl group.

Next, TD-DFT calculations were performed to investigate the excited-state properties of **Cu-2** to gain a better understanding of the photoinduced radical generation process (Extended Data Fig. 2c). The vertical excitation energy from the ground state to the S_1 state was calculated to be 88.7 kcal/mol (3.85 eV). Relaxation of the initially excited state leads to the S_1 state minimum **I-S_1**, which lies 66.1 kcal/mol above the ground state of **Cu-2**. From **I-S_1**, rapid C–S bond cleavage occurs via **TS-1-S_1** with a Gibbs free-energy barrier of only 4.1 kcal/mol, generating a CF_3 radical and the Cu(II) complex **Int-Cu^{II}** (Extended Data Fig. 2c). Finally, the photodecomposition quantum yield of **Cu-2** was experimentally determined to be 0.03 (see SI), indicating that most photoexcited **Cu-2** molecules return to the ground state, whereas a fraction enters the fragmentation pathway and is irreversibly removed from the photophysical cycle (Figure 1a, iii). Repeated excitation therefore leads to cumulative photodecomposition of **Cu-2**. Together with the light on/off experiments (Fig. 2f), this low quantum yield also rules out an efficient radical-chain propagation mechanism as the dominant pathway. Taken together, these results support that the ligand fragmentation redirects MLCT excitation toward irreversible C–S bond cleavage and radical generation.

A broad range of alkyl sulfones was next examined to assess the generality of this MLCT-enabled radical generation platform (Fig. 3a). Heteroaryl alkyl sulfones with reduction potentials ranging from −2.27 to −1.51 V all underwent efficient radical generation under the standard conditions. In contrast, the corresponding trifluoromethyl aryl sulfone (**1n**), with a more favorable reduction potential (E = −1.42 V), failed to generate any detectable trifluoromethyl radicals upon 450 nm irradiation in the presence of an equimolar amount of **Cu-1**, presumably due to the lack of a suitable coordination site in **1n** (Fig. S2). These results demonstrate that radical generation is not dictated by the reduction potential of the free sulfone alone, but

ACCELERATED ARTICLE PREVIEW

depends critically on its ability to coordinate to the copper center. Representative transformations, including alkylation of alkenes (Fig. 3b), alkene difunctionalization (Fig. 3c) and fluoroalkylation of arenes (Fig. 3d) and alkynes (Fig. 3e), further highlight its synthetic utility. The catalytic use of copper in the latter reactions (Figs. 3d and 3e) underscores the potential of this MLCT-enabled platform for developing new metal-catalyzed synthetic methods (the proposed mechanisms are illustrated in Figs. S13 and S16, respectively). Despite these advances, we sought to leverage this platform to address a more challenging and synthetically underdeveloped problem.

Cyclobutyl-containing molecules have recently emerged as important motifs in medicinal chemistry[28-31]. However, the incorporation of perfluorocyclobutyl groups remains a longstanding challenge. Although perfluorocyclobutyl iodide (**I-FCB**), a key precursor to this motif, was reported more than half a century ago (Fig. 4a)[32], the strong electron-withdrawing nature of the perfluorocyclobutyl group renders **I-FCB** an exceptionally electrophilic iodinating reagent, prone to rapid decomposition in the presence of nucleophiles such as iodide (Fig. 4b, top). In addition, the corresponding perfluorocyclobutyl radical is susceptible to unselective hydrogen atom transfer (HAT) pathways (Fig. 4b, bottom)[33]. These intrinsic limitations prompted us to pursue an atom-transfer radical addition (ATRA) strategy[34-36] for perfluorocyclobutyl incorporation.

Fig. 4 | **Synthesis and reactivity investigation of perfluorocyclobutyl iodide** (**I-FCB**). **a**, Synthesis of perfluorocyclobutyl iodide. **b**, Reactivity of perfluorocyclobutyl iodide. **c**, Optimization of the perfluorocyclobutylation-iodination of alkenes; **d**, Competition between **Cu-2** and **I-FCB**. CH_3CN, acetonitrile; TMS, trimethylsilyl; AIBN, azobisisobutyronitrile; N.D., not detected; Conv., conversion.

Conventional initiation methods, however, were less efficient under the examined conditions (Fig. 4c, entries 1–3): thermal initiators and standard radical protocols afforded low yields, whereas photocatalytic conditions delivered only moderate efficiency, likely due to iodide accumulation in the reaction medium (Fig. 4c, entry 4). Given that the C–I bond in CF_3I is stronger

ACCELERATED ARTICLE PREVIEW

than that in **I-FCB** (Table S9), we envisaged that trifluoromethyl radicals could serve as competent initiators for this ATRA process. Crucially, our irreversible MLCT platform enables the preferential generation of exceptionally clean trifluoromethyl radicals independent of the intrinsic reduction potentials of substrates, while the resulting Cu–sulfinate complex (**Cu-3**) remains inert toward **I-FCB** (Fig. S4). Consistent with this design, the use of **Cu-2** as a photochemical initiator enabled efficient perfluorocyclobutylation–iodination of alkenes, delivering the desired products in yields of up to 88% (Fig. 4c, entry 5). Control experiments demonstrated that 450 nm irradiation alone (in the absence of **Cu-2**) was insufficient to initiate the reaction (Fig. 4c, entry 6), and no reaction occurred in the absence of light (Fig. 4c, entry 7).

Fig. 5 | **Scope of the reaction with various alkenes**. **31** (0.4 mmol, 1.0 equiv), **I-FCB** (0.48 mmol, 1.2 equiv), CH_2Cl_2 (4.0 mL). [a]5.0 mmol, scale, 12 h; [b]0.2 mmol scale. [c]5 mol% Et_3B/air as the initiator. *d.r.*, diastereomeric ratio.

We next evaluated two widely used initiation approaches, including amine-mediated XAT and iron-radical-mediated XAT. Both approaches afforded the desired product in less than 40% yields (Fig. S17). We attribute their limited efficiency to the generation of reducing intermediates, which enable an undesired intermolecular SET with **I-FCB** (generating the destructive iodide anion; Fig 4b, top) alongside the desired halogen-atom transfer (XAT) process. In contrast, our initiation strategy avoids generating the strongly reducing or nucleophilic species that cause unproductive decomposition of **I-FCB**, so that **I-FCB** is activated predominantly through XAT. This mechanistic rationale is further supported by our experimental observations. Under the standard conditions, 94% of **Cu-2** was consumed, whereas only 10% of **I-FCB** was consumed when the two components were reacted in equimolar amounts; concurrently, approximately 10% CF_3I was detected. As CF_3I is a characteristic product of CF_3 radical-mediated XAT, these results support the conclusion that **I-FCB** consumption occurs predominantly through XAT rather than SET reduction (Fig. 4d).

ACCELERATED ARTICLE PREVIEW

The scope and generality of the transformation were next evaluated (Fig. 5). Using model substrate **31a**, the reaction could be readily performed on a 5 mmol scale without any appreciable loss in efficiency, underscoring its practical robustness. A broad range of functional groups was well tolerated, including ethers (**33**), aryl bromides (**34**), esters (**35**), phenols (**37**), *N*-Boc-protected amines (**38**), amides (**39**), silanes (**40**), silyl ethers (**41**), acetals (**42**) and ketones (**43**). Notably, substrates bearing free hydroxyl (**44**) and carboxylic acid (**45**) groups were also compatible, delivering the desired products in excellent yields. In addition to terminal alkenes, both 1,1-disubstituted (**46**) and internal alkenes (**47**) proved to be viable substrates under the standard conditions. The utility of this method is further demonstrated by its application to the late-stage functionalization of structurally complex molecules, including Febuxostat (**48**), Eugenol (**49**), Caryophyllene oxide (**50**, via radical β-scission of the cyclobutane ring), Alibendol (**51**), Quinine (**52**) and Paclitaxel (**53**). For complex natural products (**51**–**53**), the yields obtained under conventional initiation conditions (Et_3B/air) were substantially lower than those achieved under our standard conditions, further underscoring the advantage of our irreversible MLCT platform. Subsequently, the synthetic versatility of the iodoperfluorocyclobutyl motif was explored (Extended Data Fig. 3a). Under basic conditions, it underwent dehydrohalogenation to afford alkene **54** in 69% yield. Reduction with $NaBH_4$ proceeded with near-complete conversion to give **55**, albeit in 23% isolated yield due to its low boiling point. Nucleophilic substitution with sodium azide furnished azide **56** (39%). Under photochemical conditions, borylation delivered 57 in 60% yield. In addition, radical coupling with TEMPO in the presence of $(TMS)_3SiH$ afforded adduct **58** in 53% yield. Finally, thiolation with sodium thiophenolate provided **59** in 60% yield.

Modulation of lipophilicity (log P) is a key determinant in pharmaceutical and agrochemical discovery, and strategic fluorine incorporation has long been exploited as an effective approach to fine-tune this parameter[37]. Accordingly, we determined the log P values of a series of alkanes bearing distinct fluorinated substituents (**54**, **55**, **60**–**62**) using C18 reverse-phase HPLC (Extended Data Fig. 3b)[38,39]. Notably, the perfluorocyclobutyl motif (**54**, **55**) displayed the highest lipophilicity, marginally exceeding that of the heptafluoroisopropyl group (**61**), despite both containing the same number of fluorine atoms, and exhibiting a markedly higher log P than the perfluorocyclopropyl analogue (**62**).

ACCELERATED ARTICLE PREVIEW

Data availability

All data are available in the main text or the Supplementary Information (SI).

References

1. Prier, C. K., Rankic, D. A., MacMillan, D. W. C. Visible light photoredox catalysis with transition metal complexes: applications in organic synthesis. *Chem. Rev*. **113**, 5322–5363 (2013).
2. Chan, A. Y., Perry, I. B., Bissonnette, N. B., Buksh, B. F., Edwards, G. A., Frye, L. I., Garry, O. L., Lavagnino, M. N., Li, B. X., Liang, Y., Mao, E., Millet, A., Oakley, J. V., Reed, N. L., Sakai, H. A., Seath, C. P., MacMillan, D. W. C. Metallaphotoredox: The merger of photoredox and transition metal catalysis. *Chem. Rev*. **122**, 1485–1542 (2022).
3. Kunkely, H., Vogler, A. Photochemistry of nitratobis(triphenylphosphine)copper(I). *J. Am. Chem. Soc.* **117**, 540–541 (1995).
4. Kunkely, H., Vogler, A. Photoreduction of carbonate in a copper(I) complex. *Inorg. Chem. Commun.* **13**, 137–138 (2010).
5. Vogler, A., Kunkely, H. Photoreactivity of metal-to-ligand charge transfer excited states. *Coord. Chem. Rev*. **177**, 81–96 (1998).
6. Qin, J., Li, Y., Hu, Y., Huang, Z., Miao, W. & Chu, L. Photoinduced nickel-catalyzed homolytic C(sp^3)–N bond activation of isonitriles for selective carbo- and hydro-cyanation of alkynes. *J. Am. Chem. Soc.* **146**, 27583–27593 (2024).
7. Sinha, N., Wenger, O. S. Photoactive metal-to-ligand charge transfer excited states in $3d^6$ complexes with Cr^0, Mn', Fe", and Co^{III}. *J. Am. Chem. Soc.* **145**, 4903–4920 (2023).
8. An, Q. Chang, L. Pan, H. Zuo, Z. Ligand-to-metal charge transfer (LMCT) catalysis: harnessing simple cerium catalysts for selective functionalization of inert C−H and C−C bonds. *Acc. Chem. Res*. **57**, 2915−2927 (2024).
9. Yang, Y. Huang, X. Jin, Y. Photoinduced ligand-to-metal charge transfer (LMCT) in organic synthesis: reaction modes and research advances. *Chem. Commun.,* **61***,* 1944–1961 (2025).
10. Lima, C. G. S., Lima, T. de M., Duarte, M., Jurberg, I. D., Paixão, M. W. Organic synthesis enabled by light-irradiation of EDA complexes: theoretical background and synthetic applications. *ACS Catal.* **6**, 1389–1407 (2016).
11. Crisenza, G. E. M., Mazzarella, D., Melchiorre, P. Synthetic methods driven by the photoactivity of electron donor–acceptor complexes. *J. Am. Chem. Soc.* **142**, 5461–5476 (2020).
12. Buzzetti, L., Prieto, A., Roy, S. R., Melchiorre, P. Radical-based C–C bond-forming processes enabled by the photoexcitation of 4-alkyl-1,4-dihydropyridines. *Angew. Chem. Int. Ed.* **56**, 15039–15043 (2017).
13. Sato, Y., Nakamura, K., Sumida, Y., Hashizume, D., Hosoya, T. & Ohmiya, H. Generation of alkyl radical through direct excitation of boracene-based alkylborate. *J. Am. Chem. Soc.* **142**, 9938–9943 (2020).
14. Rong, J., Deng, L., Tan, P., Ni, C., Gu, Y. Hu, J. Radical fluoroalkylation of isocyanides with fluorinated sulfones by visible light photoredox catalysis. *Angew. Chem. Int. Ed.* **55**, 2743–2747 (2016).
15. Wei, Z., Miao, W., Ni, C., Hu, J. Iron-catalyzed fluoroalkylation of arylborates with sulfone

ACCELERATED ARTICLE PREVIEW

reagents: beyond the limitation of reduction potential. *Angew. Chem. Int. Ed*. **60**, 13597–13602 (2021).
16. Viradiya, R. H., Choudhary, A., Morja, M. & Chikhlia, K. H. General overview on recent advance in light-induced Cu-I/II photoredox catalysis without metal co-catalyst. *Chem. Eng. Process Tech.* **9**, 1095 (2024).
17. Kainz, Q. M., Matier, C. D., Bartoszewicz, A., Zultanski, S. L., Peters, J. C., Fu, G. C. Asymmetric copper-catalyzed C–N cross-couplings induced by visible light. *Science* **351**, 681–684 (2016).
18. Dong, X.-Y., Zhang, Y.-F., Ma, C.-L., Gu, Q.-S., Wang, F.-L., Li, Z.-L., Jiang, S.-P., Liu, X.-Y. A general asymmetric copper-catalysed Sonogashira C(sp^3)–C(sp) coupling. *Nat. Chem*. **11**, 1158–1164 (2019).
19. Dong, X.-Y., Li, Z.-L., Gu, Q.-S., Liu, X.-Y. Ligand development for copper-catalyzed enantioconvergent radical cross-coupling of racemic alkyl halides. *J. Am. Chem. Soc.* **144**, 17319–17329 (2022).
20. Chen, C., Fu, G. C. Copper-catalyzed enantioconvergent alkylation of oxygen nucleophiles. *Nature* **618**, 301–307 (2023).
21. Beaudelot, J. *et al.* Photoactive copper complexes: properties and applications. *Chem. Rev.* **122**, 16365–16609 (2022).
22. Ouyang, Y., Xu, X.-H., Qing, F.-L. Electrochemical trifluoromethoxylation of (hetero)aromatics with a trifluoromethyl source and oxygen. *Angew. Chem. Int. Ed.* **61**, e202114048 (2022).
23. Brown, C. M. et al. Influence of sulfur oxidation state and substituents on sulfur-bridged luminescent copper(I) complexes showing thermally activated delayed fluorescence. *Inorg. Chem.* **58**, 7156–7168 (2019).
24. Delaney, C. P. et al. Cross-coupling by a noncanonical mechanism involving the addition of aryl halide to Cu(II). *Science* **381**, 1079–1085 (2023).
25. Luo, Y. et al. Decoding the redox behaviour of copper in Ullmann-type coupling reactions. *Nature* **646**, 1105–1113 (2025).
26. Babgi, B. A. Synthetic protocols and applications of copper(I) phosphine and copper(I) phosphine/diimine complexes. *J. Organomet. Chem.* **956**, 122124 (2021).
27. Liu, Z., Lu T., Chen Q. An sp-hybridized all-carboatomic ring, cyclo[18]carbon: Electronic structure, electronic spectrum, and optical nonlinearity. *Carbon* **165**, 461–467 (2020).
28. Bauer, M. R., Di Fruscia, P., Lucas, S. C. C., Michaelides, I. N., Nelson, J. E., Storer, R. I. Whitehurst, B. C. Small aliphatic rings in medicinal chemistry. *RSC Med. Chem.* **12**, 448–471 (2021).
29. Ren, S., Pan, F., Zhang, W., Rao, G.-W. Molecules containing cyclobutyl fragments as therapeutic tools: a review on cyclobutyl drugs. *Curr. Med. Chem.* **29**, 4113–4135 (2022).
30. Shah, A., Hayes, C. J., Martin, B. C. Characteristics of initial prescription episodes and likelihood of long-term opioid use — United States, 2006–2015. *MMWR Morb. Mortal. Wkly. Rep.* **66**, 265–269 (2017).
31. Dhillon, S. Ivosidenib: first global approval. *Drugs* **78**, 1509–1516 (2018).
32. Krespan, C. G. Synthesis of fluoroalkyl iodides. *J. Org. Chem.* **27**, 1813–1814 (1962).
33. Hell, S. M., Meyer, C. F., Ortalli, S., Sap, J. B. I., Chen, X., Gouverneur, V. Hydrofluoromethylation of alkenes with fluoroiodomethane and beyond. *Chem. Sci.* **12**, 12149–12158 (2021).

ACCELERATED ARTICLE PREVIEW

34. Engl, S., Reiser, O. Copper-photocatalyzed ATRA reactions: concepts, applications, and opportunities. *Chem. Soc. Rev.* **51**, 5287–5299 (2022).
35. Reichle, A., Koch, M., Sterzel, H., Großkopf, L.-J., Floss, J., Rehbein, J., Reiser, O. Copper(I) photocatalyzed bromonitroalkylation of olefins: evidence for highly efficient inner-sphere pathways. *Angew. Chem. Int. Ed.* **62**, e202219086 (2023)
36. Mandal, T., Ghosh, M., Paps, H., Mandal, T., Reiser, O. A general photocatalytic platform for the regio- and stereoselective β-chloroacylation of alkenes and alkynes using a heteroleptic copper(I) complex. *Nat. Catal.* **8**, 607–622 (2025).
37. Jeffries, B., Wang, Z., Felstead, H. R., Le Questel, J.-Y., Scott, J. S., Chiarparin, E., Graton, J., Linclau, B. Systematic investigation of lipophilicity modulation by fluorination in medicinal chemistry. *J. Med. Chem.* **63**, 1002–1031 (2020).
38. Xu, W., Xu, X., Qing, F.-L. Fluorinated motifs and their impact on molecular properties. *Chin. J. Chem.* **38**, 847–854 (2020).
39. Thomson, C. J., Zhang, Q., Al-Maharik, N., Bühl, M., Cordes, D. B., Slawin, A. M. Z., O'Hagan, D. Conformational and lipophilicity effects of fluorinated substituents. *Chem. Commun.* **54**, 8415–8418 (2018).

Acknowledgements

We acknowledge Dr. Menghui Jia (ECNU) for conducting the transient absorption spectrum (TAS) experiments and data processing, and Dr. Ruihua Pu (ShanghaiTech University) for his assistance in the TAS data interpretation.

Funding

We are grateful to the financial support provided by the National Natural Science Foundation of China (22261132514, 22271299, and 22625303), the Strategic Priority Research Program of the Chinese Academy of Sciences (XDB0590000), and the National Key R&D Program of China (2025YFA1511100).

Author contributions

J.H. and Z.W. conceived the work. Z.W., X.L., L.X. and Y.H. performed the reaction optimization, reaction scope examination and mechanistic studies. X.-S.X. designed and directed computational studies, and Z.L. and K.Z. performed computational studies. C.N. contributed to the study of copper-sulfone complexes and perfluorocyclobutylation reactions. J.H. directed the whole study. All authors contributed to the writing of the manuscript.

Competing interests

ACCELERATED ARTICLE PREVIEW

The authors declare no competing interests.

Additional information

Supplementary Information is available for this paper at…

Reprints and permissions information is available at www.nature.com/reprints.

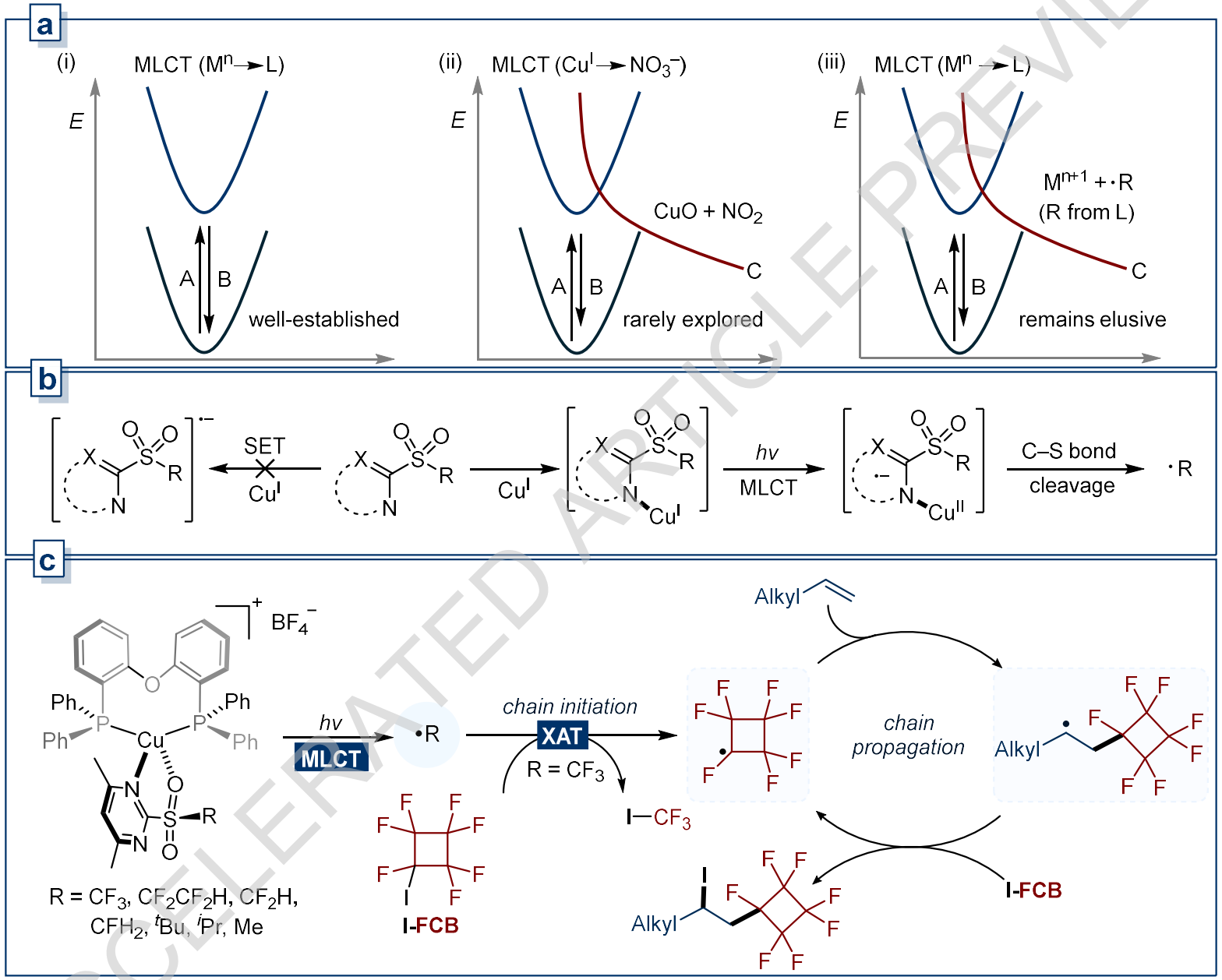
Correspondence and requests for materials should be addressed to J.H. (jinbohu@sioc.ac.cn; for experimental studies) or X.-S.X. (xuexs@sioc.ac.cn; for computational studies).

Extended Data Fig. 1 | **Structural and EPR characterization of Cu complexes**. **a**, Single-crystal X-ray structure of **Cu-1**. **b**, Single-crystal X-ray structure of **Cu-2**. **c**, EPR spectrum of **Int-Cu^{II}**. **d**, Single-crystal X-ray structure of **Cu-3**.

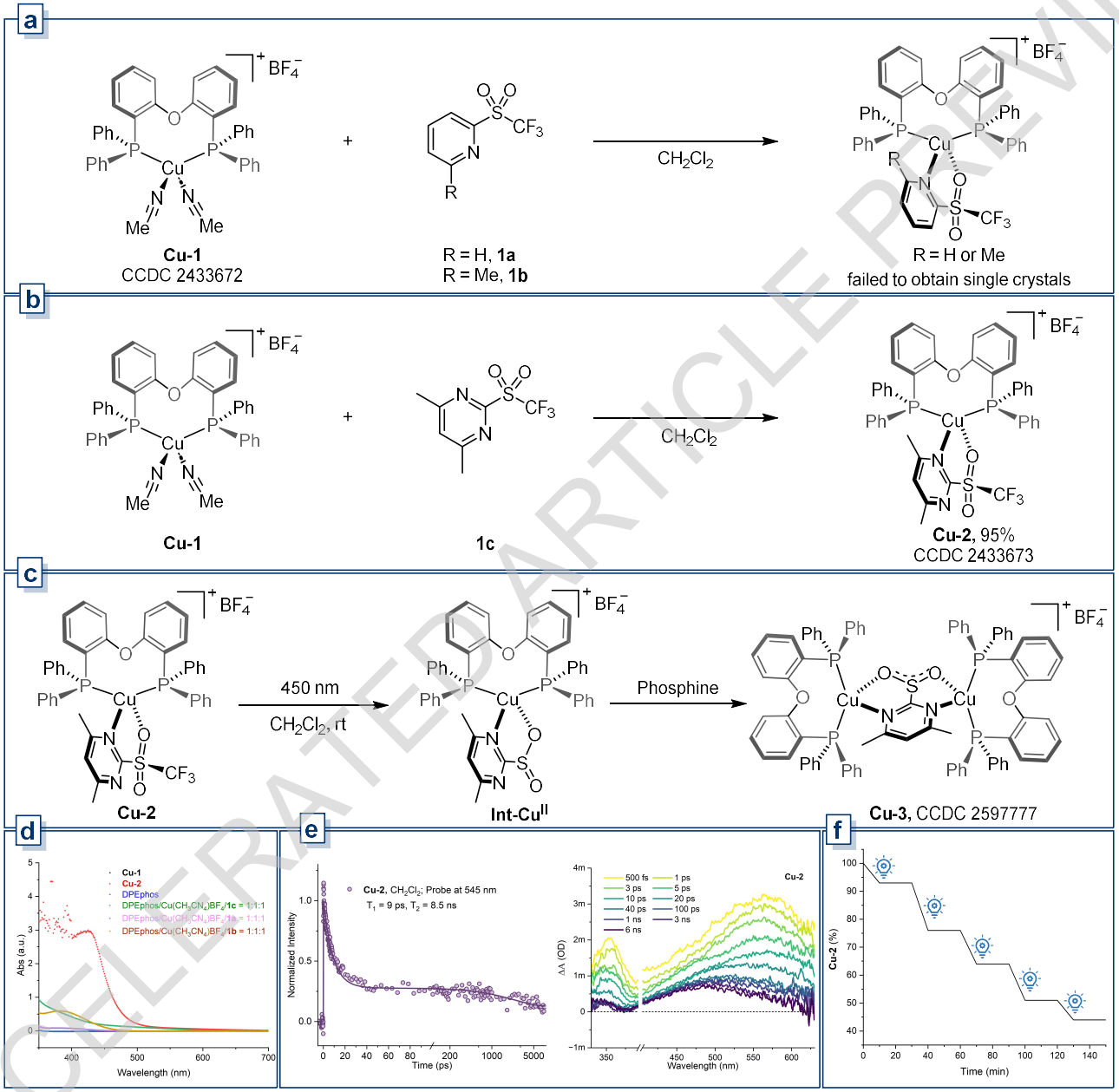
Extended Data Fig. 2 | **DFT and TD-DFT calculations on the excited state of Cu-2**. **a**, Population of frontier orbitals of **Cu-2**. **b**, Hole-electron analysis of S_1 state **Cu-2**-S_1. **c**, Energy profiles of photoinduced generation of CF_3 radical from **Cu-2**. HOMO, Highest Occupied Molecular Orbital; LUMO, Lowest Unoccupied Molecular Orbital.

Extended Data Fig. 3 | **Synthetic applications. a**, Product transformations. **b**, Log *P* values of various fluoroalkylated molecules.

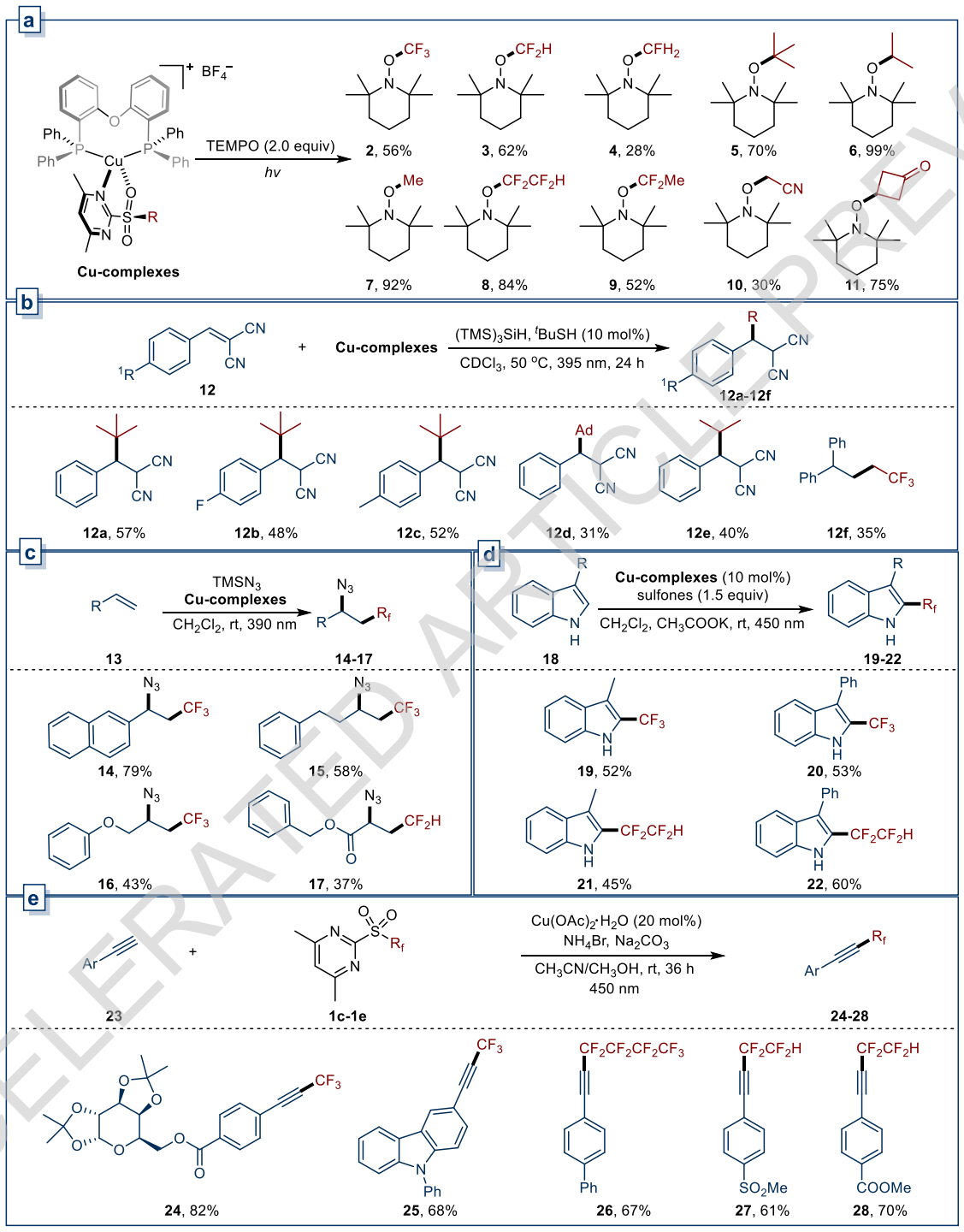
ACCELERATED ARTICLE PREVIEW



ACCELERATED ARTICLE PREVIEW

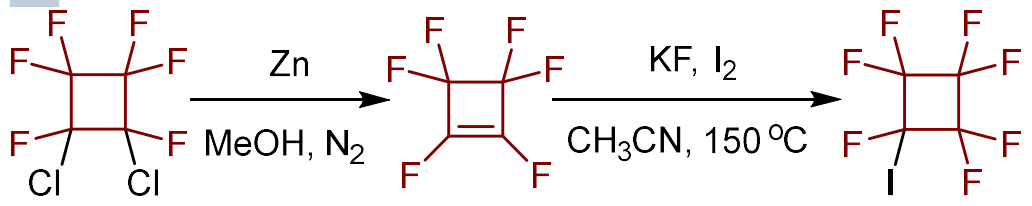


ACCELERATED ARTICLE PREVIEW



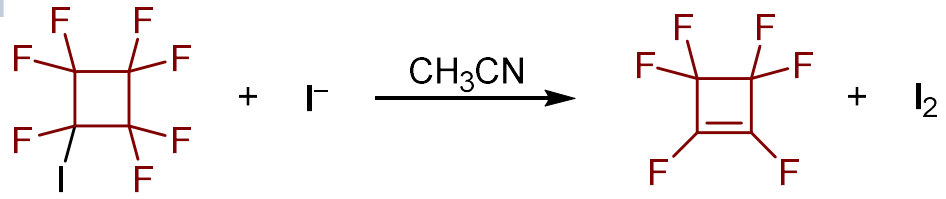
ACCELERATED ARTICLE PREVIEW

a

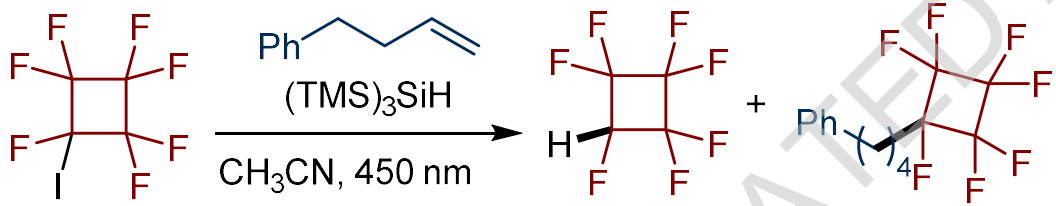


3a **FCB**, 91% **I-FCB** 26%, 12.8 g

b

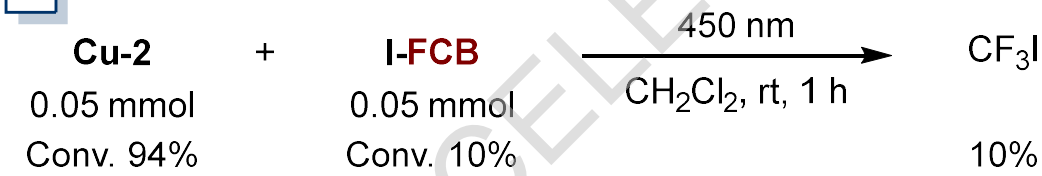


I-FCB **FCB**

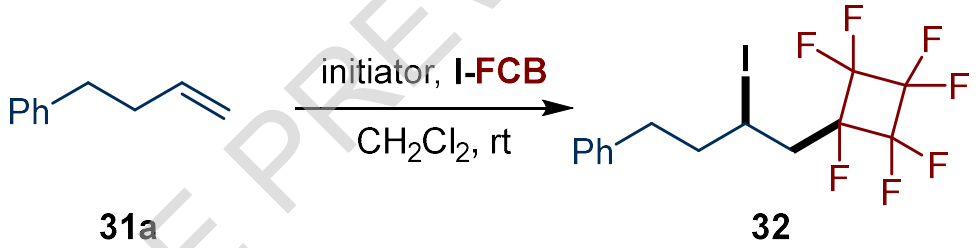


I-FCB 52% N.D.

d



c

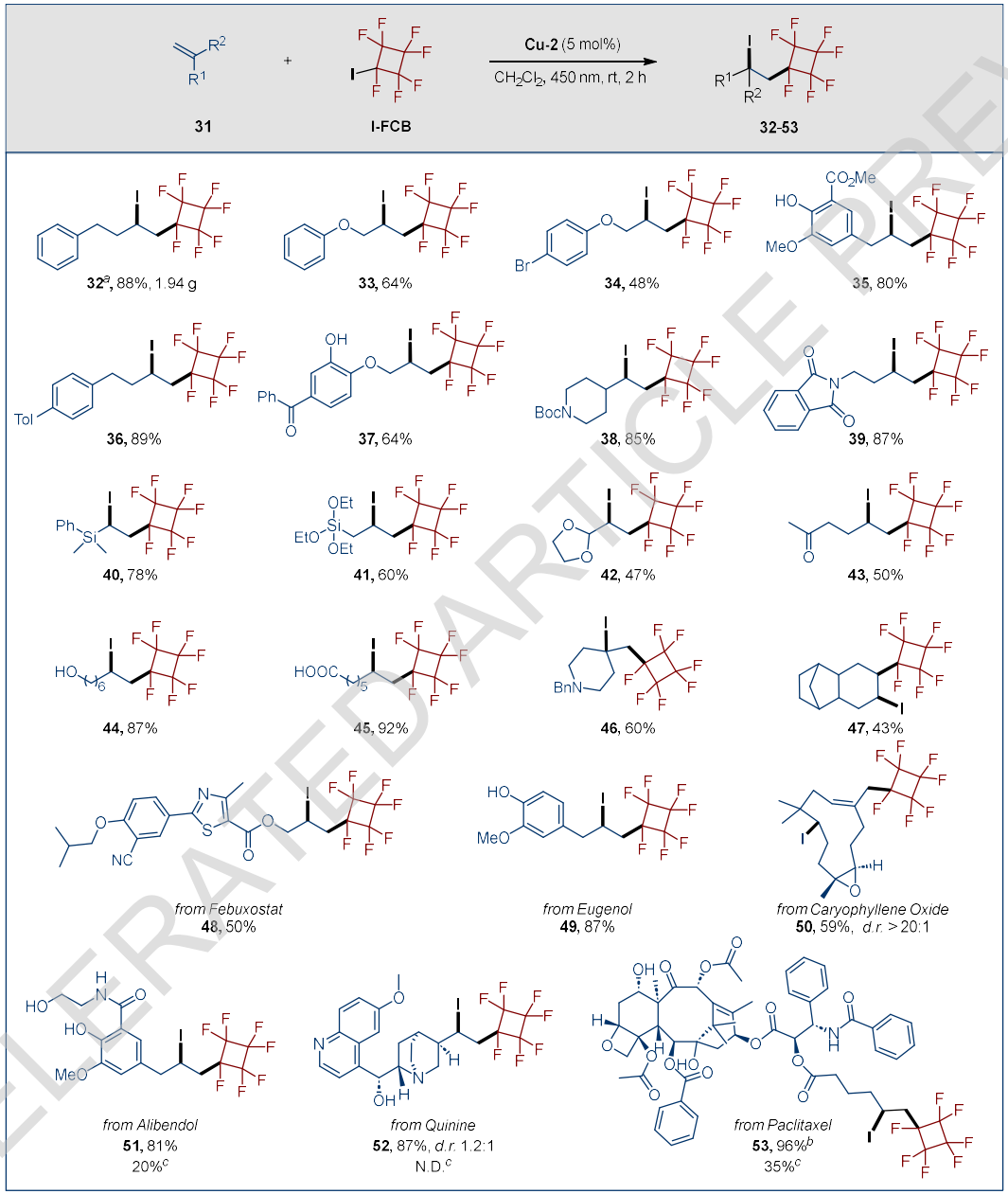


31a **32**

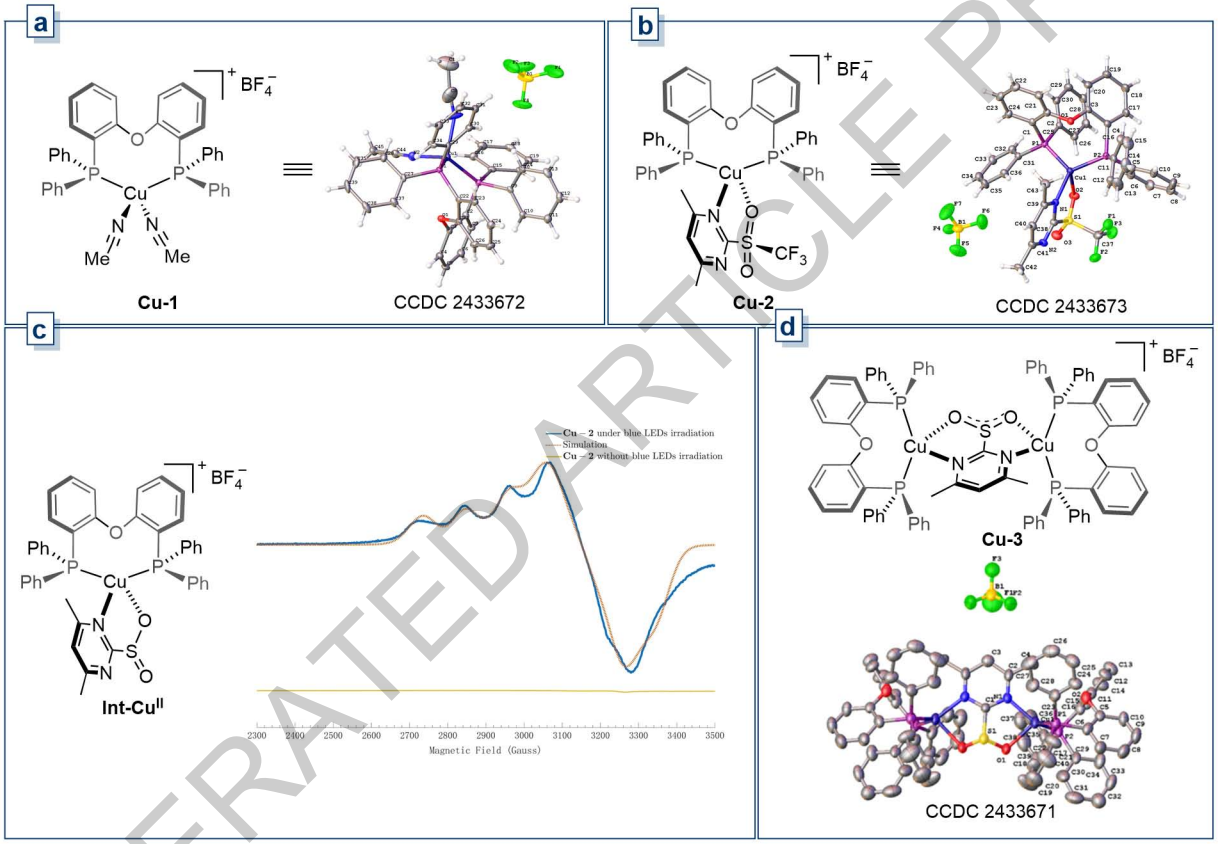
entry	initiator	yield (%)
1[a]	AIBN (10 mol%)	N.D.
2[a]	AIBN and Bu_3SnH (10 mol%)	25
3	Et_3B (5 mol%), air	49
4[b]	**Cu-1** (5 mol%)	54
5[b]	**Cu-2** (5 mol%)	88
6[b]	-	N.D.
7[c]	**Cu-2** (5 mol%)	N.D.

[a]Toluene as solvent, 90 °C; [b]450 nm irradiation; [c]No light.

ACCELERATED ARTICLE PREVIEW

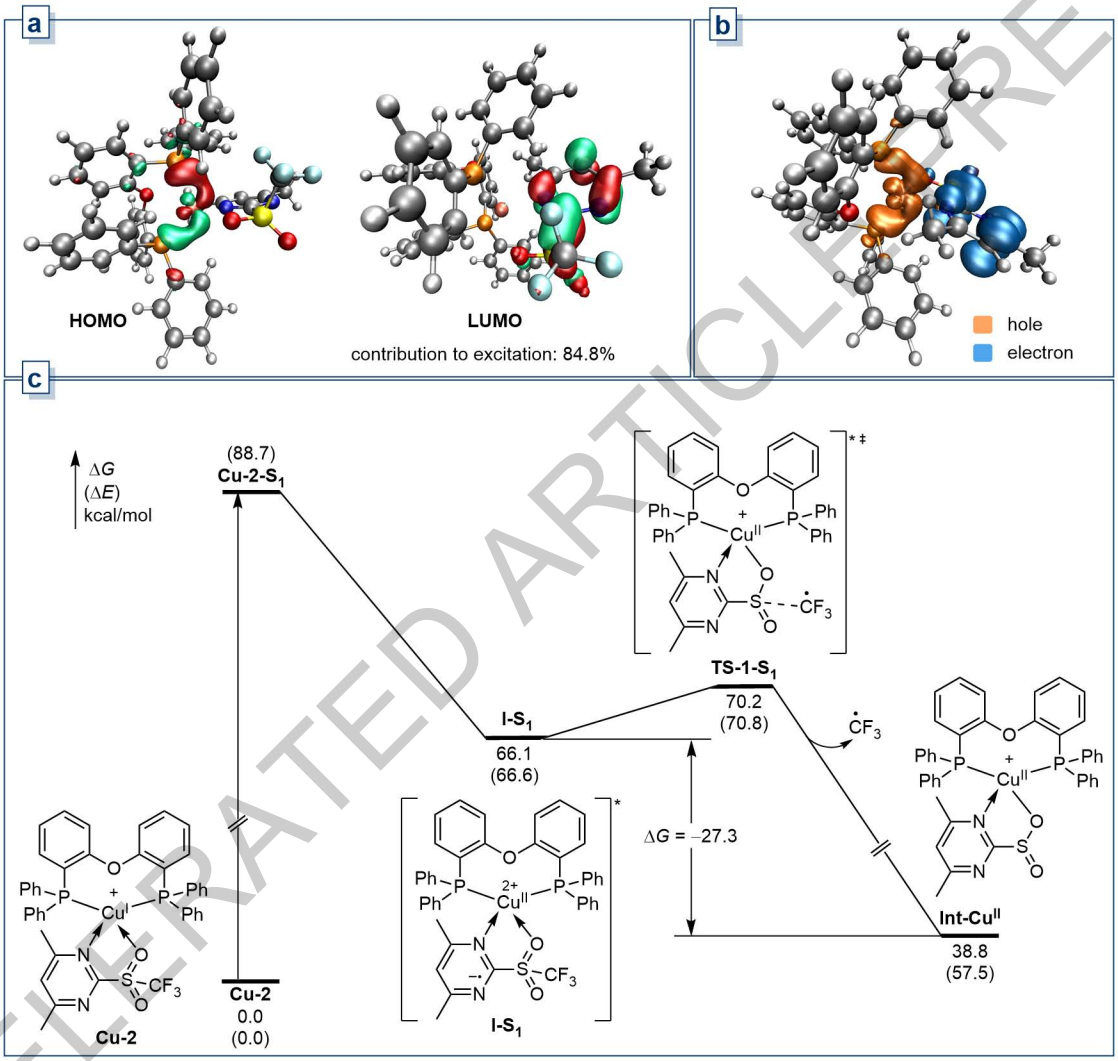


ACCELERATED ARTICLE PREVIEW



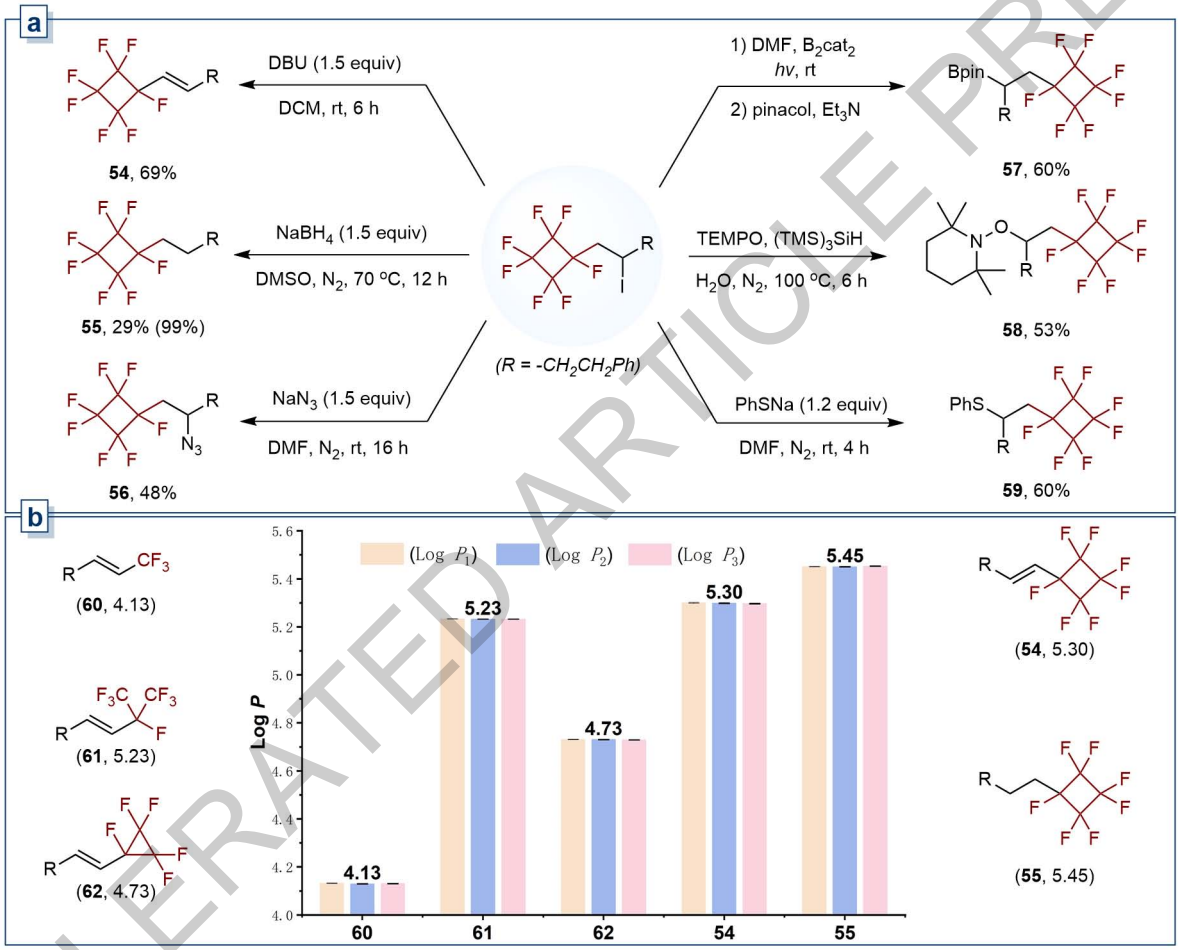
Extended Data Fig. 1

ACCELERATED ARTICLE PREVIEW



Extended Data Fig. 2

ACCELERATED ARTICLE PREVIEW



Extended Data Fig. 3

ACCELERATED ARTICLE PREVIEW